JTTEE5 4:75-84

Quenching Stress in Plasma Sprayed Coatings and Its Correlation with the Deposit Microstructure

S. Kuroda, T. Dendo, and S. Kitahara

Quenching stress arises within a thermally sprayed splat as its thermal contraction after solidification is constrained by the underlying solid. Dependence of the quenching stress in plasma-sprayed deposits of Ni-20Cr alloy and alumina on the substrate temperature during spraying was discussed in conjunction with the change in the nature of the interlamellar contact between splats. It was found by mercury intrusion porosimetry and observation of cross sections of impregnated deposits that the interlamellar contact is improved significantly by raising the substrate temperature during deposition from 200 to 600 °C. The positive dependence of the quenching stress on the substrate temperature in this temperature range was attributed to a stronger constraint against thermal contraction of sprayed splats after solidification due to the improved contact.

1. Introduction

UNDER typical plasma spray conditions, powder particles in the size range of 10 to 100 μm in a molten state strike the substrate at a velocity over 100 m/s. As shown in Fig. 1, each droplet spreads and quenches during a very short time in the order of 1 to 10 μs, resulting in a very fine microstructure within a splat, which is characteristic of rapidly solidified materials. As the splat cools further after solidification, its thermal contraction is constrained by the underlying solid, and an in-plane tensile stress, the so called "quenching stress," is developed in the splat. The quenching stress is not only a unique and important source of the residual stresses in thermally sprayed deposits but also has significant implications for the deposit formation as discussed.

Recently the development of an instrument to measure the substrate curvature in situ during spraying has made it possible to determine the average value of quenching stress in a large number of splats (Ref 1). The results obtained are summarized as follows (Ref 2-4).

Quenching stress becomes independent of the substrate material and its surface pretreatment as soon as the coating thickness exceeds approximately 10 μm. Thereafter, the steady-state value of quenching stress is a function of the characteristics of the impinging particles and the substrate temperature only.

Then, the dependence of the steady-state quenching stress of a wide range of powder materials on substrate temperature was studied. Generally the values of quenching stress of soft fcc metals, such as Ni and Al, are below 100 MPa and tend to decrease with the substrate temperature, whereas the values for alloys with excellent high-temperature strength tend to be high (even over 300 MPa) and exhibit a positive dependence on the substrate temperature first and then decrease at a sufficiently high temperature. For ceramics, the quenching stress is usually very small (less than 50 MPa) because the stress is effectively relieved by intensive microcracking.

From the dependence of the quenching stress on the substrate temperature and the thermal and mechanical properties of the sprayed materials, several stress relaxation mechanisms have been proposed to occur during rapid cooling after solidification. They include plastic yielding, creep, surface relaxation due to the edge effect, microcracking, and interfacial sliding due to imperfect bonding between splats.

Another line of important progress was made by Gill and Clyne (Ref 5-7). They constructed a numerical model that incorporates the macroscopic thermal and mechanical behavior of a coating and substrate couple during plasma spray, including the quenching stress determined experimentally, to calculate the through-thickness stress distribution during and after deposition. The model has been verified by comparing the calculated change in the substrate curvature during deposition with the experimental curve obtained by an analysis of video images. The technique was extended by Howard and Clyne to evaluate the interfacial toughness between a sprayed coating and the substrate (Ref 8).

In a previous paper, the present authors reported a strong correlation between the values of quenching stress for plasma

Keywords: residual stress, porosity, interlamella contact, substrate temperature, rapid solidification

S. Kuroda, T. Fukushima, and **S. Kitahara,** National Research Institute for Metals, Advanced Materials Processing Division, 1-2-1, Sengen, Tsukuba-shi, Ibaraki-ken, 305 Japan.

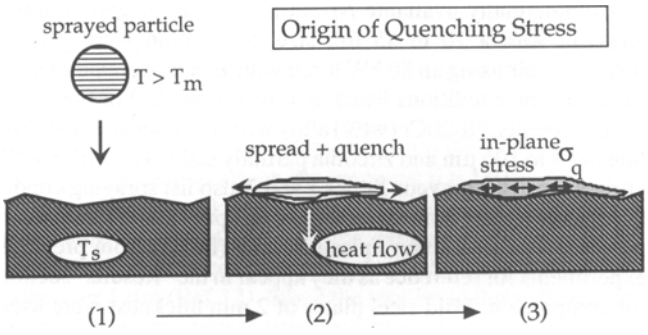

Fig. 1 Origin of quenching stress in thermal spraying.

Table 1 Atmospheric plasma spray conditions

Powder material	Powder size, μm	Plasma gas	Flow rate, L/min	Arc current	Voltage	Powder feed rate, g/min	Powder feed gas flow rate, L/min
Ni	10-45	Ar	45	600 A	30	8	2.5
Ni-20Cr (wt%)	10-45	Ar	45	600 ~ 750A	30	10	2.5
Ni-20Cr (wt%)	74-105	Ar	45	600 A	30	10	2.5
Alumina	10-45	Ar	45	600 ~ 750A	30	5	2.5
8YPSZ(a)	10-45	Ar	45	1.2 kA	30	12.5	2.5

Note: Spray distance, 100 mm; torch linear velocity 0.18 m/s. (a) ZrO_2 partially stabilized with 8 wt% Y_2O_3, fused and crushed powder.

Table 2 Low-pressure plasma spray conditions

Powder material	Powder size, μm	Primary plasma gas	Primary flow rate, L/min	Secondary plasma gas	Secondary flow rate, L/min	Arc current	Voltage	Powder feed rate, g/min	Powder feed gas flow rate, L/min
Ni	10-45	Ar	50	H_2	4	700	50	38	2.5
Ni-20Cr	10-45	Ar	50	H_2	4	700	50	26	2.5

Note: Chamber pressure, 20 kPa; spray distance, 300 mm; torch linear velocity, 0.1 m/s.

sprayed Ni-20Cr and alumina deposits and their mechanical properties, such as Young's modulus and bend strength in a range of relatively low (200 to 500 °C) substrate temperatures (T_s), where both deposits exhibited a significant positive dependence on the substrate temperature. The explanation was given by an assumption that the bonding between splats is improved at a higher substrate and coating temperature during deposition. This improved bonding will constrain more strongly the thermal contraction of each splat during cooling after solidification and result in a higher value of quenching stress. It will also provide stronger linkage among splats within a coating and result in enhanced mechanical properties of a coating.

In the present paper, microstructure of deposits plasma sprayed in air at various substrate temperatures is investigated in conjunction with measurements of the quenching stress to confirm the above assumption.

2. Experiments

2.1 *Spraying Conditions*

Commercially available Ni-20Cr (wt%) alloy and alumina powders with a 10 to 45 μm size distribution were plasma sprayed in air using an 80 kW torch with an 8 mm diameter nozzle under the conditions listed in Tables 1 and 2. For the stress measurements, Ni-20Cr (wt%) alloy with a coarser size distribution of 74 to 105 μm and zirconia partially stabilized with 8 wt% yttria were also sprayed. Tables 1 and 2 also list spraying conditions with Ni for atmospheric plasma spray (APS) and some powders for low-pressure plasma spray (LPPS) from previous experiments for reference as they appear in the "Results" section for comparison. Mild steel plates of 2 mm thickness were used as substrates for both the stress measurements and the sample preparation for the porosity measurements.

2.2 *Measurement of Quenching Stress*

Suppose a thin film was stretched, and then its surface was bonded to a substrate. The substrate would bend, and the film/substrate couple would come to an equilibrium. If the film thickness is negligible with respect to the substrate thickness, the equilibrium curvature of the substrate is proportional to the stress within the film (Ref 9). The following experimental technique is based on this principle. The curvature of a substrate was measured in situ during spraying by an instrument shown in Fig. 2, the details of which have been reported elsewhere (Ref 1). The instrument detects the bending δ of a substrate fixed onto a pair of knife edges by a contacting linear variable differential transformer (LVDT). The parameter δ is, in the first order approximation, proportional to the curvature $1/R$ of the substrate, i.e., $1/R = 8\,\delta/l^2$, where l is the span between the knife edges. From the rate of the curvature change with respect to the coating thickness, h_d, the average quenching stress, $\sigma_q(T_s)$, within splats can be determined as:

$$\sigma_q(T_s) = \frac{E_s(T_s)h_s^2}{6(1-\nu)}\frac{\delta}{\delta h_d}\left(\frac{1}{R}\right) \qquad \text{(Eq 1)}$$

where E_s, h_s, and ν are the Young's modulus, thickness, and Poisson's ratio of the substrate, respectively (Ref 9-11). In the calculation, $\nu = 0.3$, and the temperature dependence of the modulus was taken into account by a formula $E_s(T_s) = E_0\,[1 - 0.000313(T_s - 20)]$, where $E_0 = 2 \times 10^{11}$ Pa and T_s is measured in degrees centigrade.

The substrate was a 2 × 15 × 100 mm mild steel plate, which was alumina grit blasted on one of its sides and degreased in acetone before spraying. Due to the compressive stress introduced by the sand blasting, the blasted surface became convex. To avoid a possible curvature change due to the relief of the compressive stress during spraying, the blasted substrates were

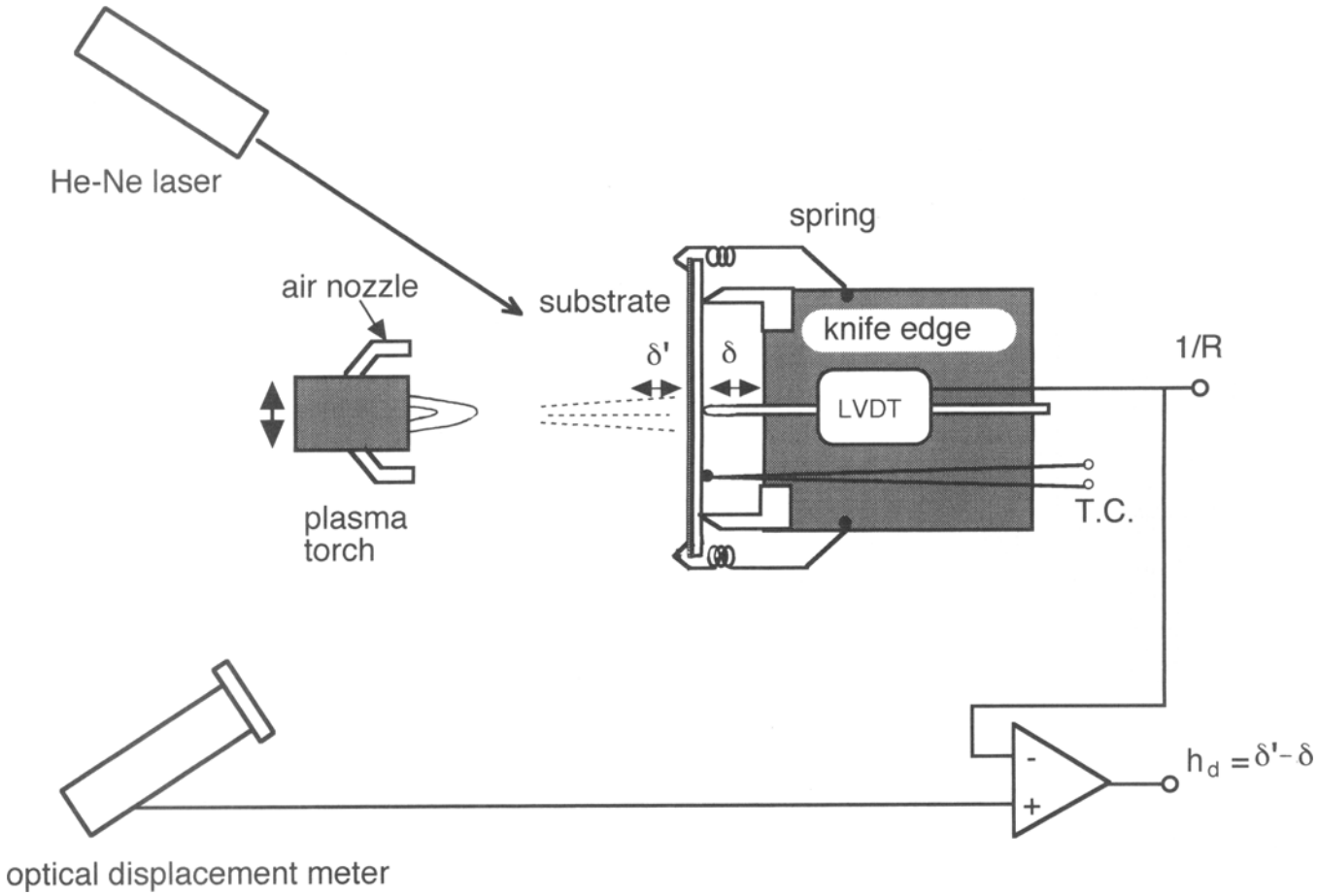

Fig. 2 *Schematic illustration of the in situ instrument to measure the curvature change of a substrate during spraying.*

either annealed in a vacuum furnace or preheated by the plasma torch prior to deposition till the substrate curvature became stable. The tension exerted by a pair of springs used to fix the substrate caused only a few microns of δ, which was negligible in most cases. Within such a thin substrate, no significant stationary thermal gradient in the thickness direction exists during spraying, and thus the curvature may be regarded as a direct measure of the quenching stress within the deposited coating as long as the average substrate temperature, T_s, is kept constant (Ref 2). The temperature of the substrate was measured by a thermocouple spot welded to the rear surface and was controlled by adjusting the flow rate of the cooling air ejected by a pair of nozzles attached to the plasma torch. The torch traversed back and forth in front of the substrate at a velocity of 0.18 m/s with a small up or down motion at the end of each traverse to form a coating with uniform thickness. The displacement δ′ of the front surface of the coating can be monitored by a laser displacement meter, and the coating thickness during deposition can be measured by $h_d = \delta' - \delta$ in situ during spraying (Ref 1).

2.3 *Porosity Measurement*

A mercury intrusion porosimeter was used to measure the size distribution of the open porosity within deposits. Coatings that were 0.7 to 2 mm thick were detached from the substrates and were further broken into pieces of approximately 7 mm × 7 mm in dimension. In order to detach the alumina coatings from the substrate, a silicone based liquid was sprayed onto the substrate surface before spraying. For the thick Ni-Cr deposits, no such treatment was necessary because the coatings tended to peel off spontaneously due to the high quenching stress of the material.

The specimens were placed in a glass cell, which was evacuated and then filled with mercury. The cell was placed in a high-pressure vessel and pressurized up to 100 MPa. The standard Washburn equation was used to convert the pressure, P, applied to mercury to the pore radius, r,

$$r = \frac{-2\gamma \cos \theta}{P} \qquad \text{(Eq 2)}$$

where the surface tension of mercury $\gamma = 0.482$ N/m and the contact angle of mercury on the specimen $\theta = 140°$.

In a previous work, it was found that when a number of thin specimens are placed in a cell, the gaps among them and between them and the cell wall can be mistaken as porosity, typically over 1 μm (Ref 12). Since the true breakthrough pressure at which mercury starts to penetrate into plasma-sprayed deposits generally corresponds to approximately 0.1 μm, the com-

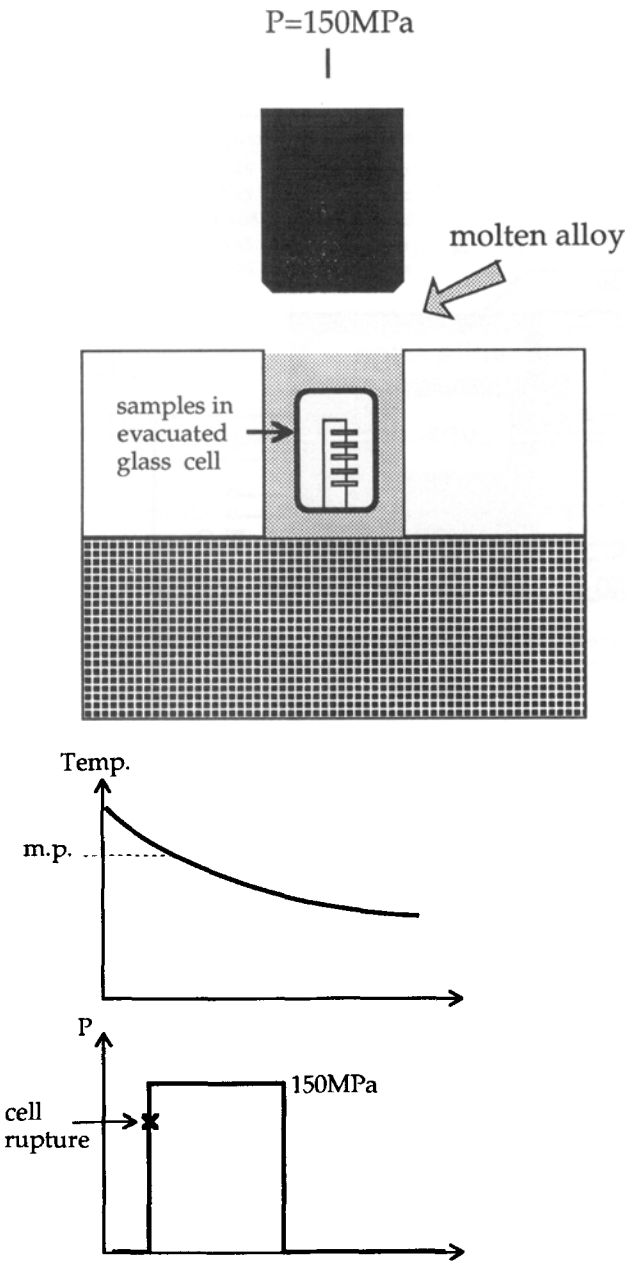

Fig. 3 Schematic illustration of the high-pressure infiltration of bismuth alloy for sprayed deposits.

bined results may appear as a bimodal size distribution. When specimens were molded in a plastic cast, this type of misinterpretation was eliminated.

2.4 *Pore Visualization by Impregnation Techniques*

Chromic acid impregnation was applied to alumina deposits, whereby a specimen is immersed in a saturated chromic acid solution and then baked in air. When this process is repeated several times, open pores become filled with Cr_2O_3. The technique was first applied successfully by Takahashi and Senda to alumina deposits plasma sprayed at different spray distances to examine the differences in the pore structures (Ref 13).

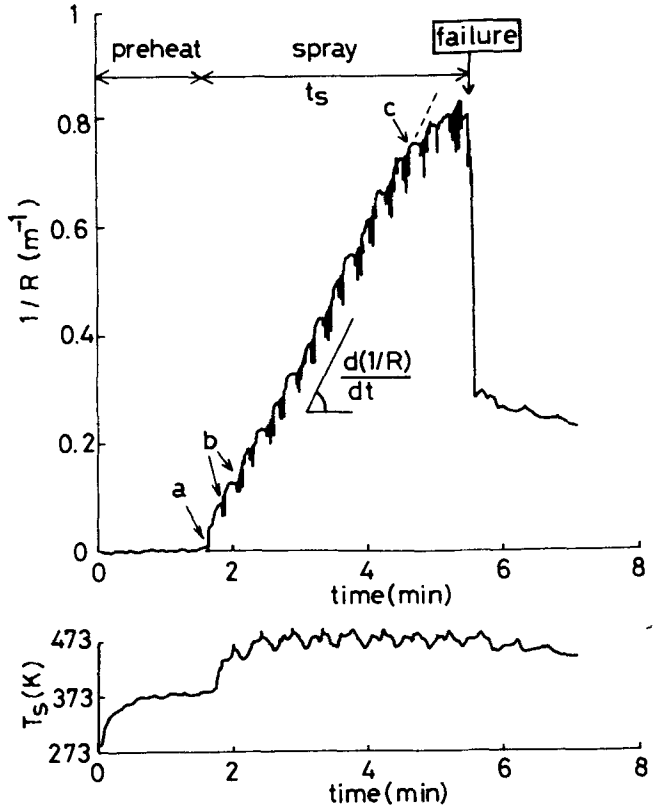

Fig. 4 Typical evolutions of the curvature and substrate temperature during spraying of Ni-20Cr powder.

High-pressure infiltration of a low melting point Bi alloy was applied to Ni-Cr deposits as shown in Fig. 3. A specimen sealed in an evacuated glass cell was placed in a crucible, to which a molten Bi alloy was poured, and a high pressure of about 150 MPa was applied thereafter. The pressure breaks the cell and forces the molten alloy to infiltrate into the deposits. After solidification, specimens were cut from the cast alloy.

After these treatments, specimens were molded in plastic to have their cross sections polished metallographically. Since the materials within the pores are composed of heavier atoms than the matrix, they can now be observed with a high contrast and spatial resolution in the back-scattered electron image under scanning electron microscopy (SEM).

3. Results

3.1 *Curvature and Stress*

Figure 4 shows a typical example of the change in the curvature of a substrate when Ni-20Cr is sprayed at approximately T_s = 200 °C (473 K). As soon as spraying was started after preheating, the sprayed surface started to bend concave at point *a*. The small periodic fluctuations at point *b*, for example, observed in $1/R$ are due to the transient thermal gradient mainly from the heat of incoming powder (Ref 1, 3). By neglecting the small

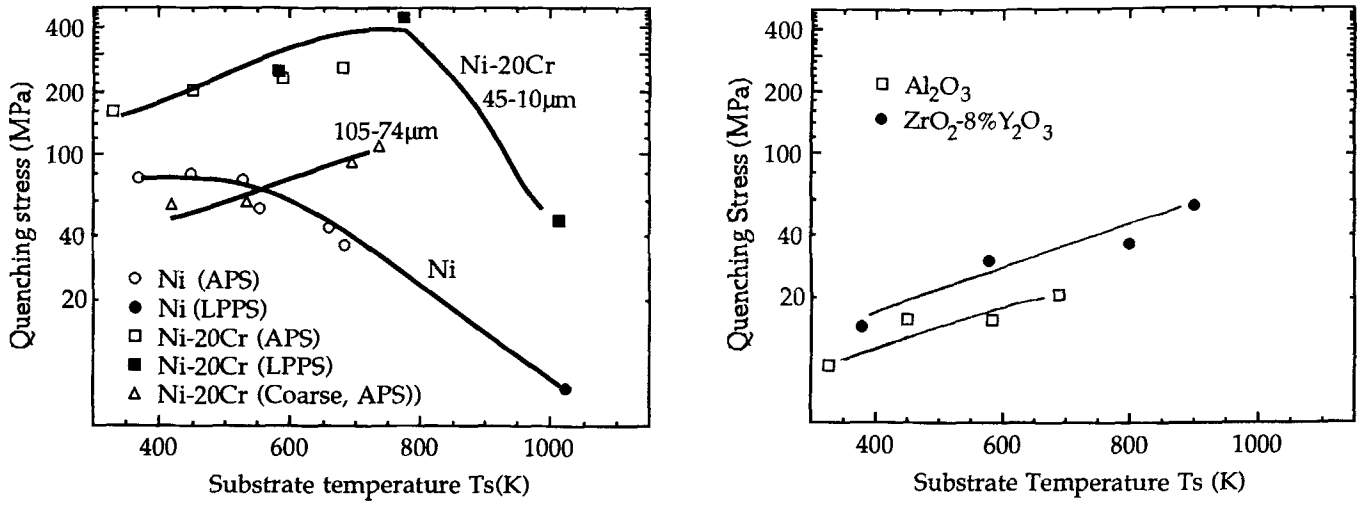

Fig. 5 Dependence of the quenching stress on substrate temperature (a) for metallic powders and (b) for ceramic powders .

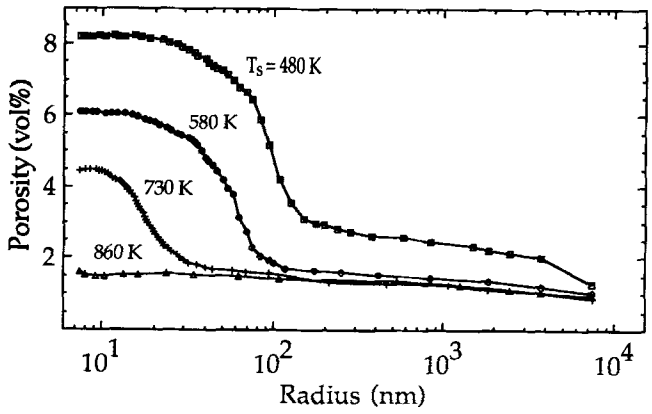

Fig. 6 Change in the pore size distribution of plasma-sprayed Ni-20Cr deposits with substrate temperature.

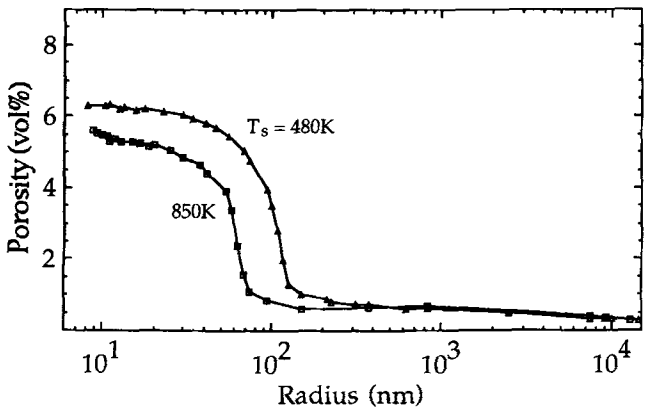

Fig. 7 Change in the pore size distribution of plasma-sprayed alumina deposits with substrate temperature.

fluctuations in the $1/R$ trace and approximating it to a straight line, one can calculate the slope, $d(1/R)/dt$, as shown in Fig. 4. The average growth rate, dh_d/dt, of the coating was calculated by dividing the final coating thickness, h_d, by the spraying time, t_s. Then $d(1/R)/dh_d$ was calculated and substituted into Eq 1 to give the average quenching stress, σ_q. As $1/R$ exceeds a certain value at point c, its rate of increase gradually decreases and finally falls rapidly, which indicates the initiation of failure at the coating/substrate interface.

The dependence of quenching stress on the substrate temperature is shown for metallic deposits in Fig. 5(a) and for ceramic deposits in Fig. 5(b). Some of the data, including the data obtained by LPPS at very high substrate temperatures, are from Ref 3 and are shown here for comparison purposes. The quenching stress of pure Ni is less than 100 MPa and decreases with T_s. In comparison, the quenching stress of Ni-20Cr alloy is well over 100 MPa, increases with the substrate temperature up to 400 MPa, and finally decreases at a temperature over 1000 K. The coarse Ni-20Cr powder (74 to 105 μm) gave significantly lower values of quenching stress compared to the 10 to 45 μm sized feedstock, probably because the degree of flattening of splats is less and the contact between splats is poorer due to the lower temperatures and velocities of powder particles on impact (Ref 14) . However, both materials exhibited a similar positive dependence on the substrate temperature in the low-temperature regime.

Quenching stresses of the two ceramic powders were significantly lower than the metallic ones, especially at lower substrate temperatures, but they also exhibited a positive dependence on T_s.

Quenching stress is expected to decline with the substrate temperature as in the case of Ni because most materials become more easily deformable at a higher temperature due to yielding and creep. However, the quenching stress of a number of materials exhibits positive temperature dependence in the ordinary range of substrate temperature for thermal spraying, especially for APS. This cannot be explained by the bulk mechanical properties; hence the bonding conditions between splats need to be examined.

3.2 *Pore Size Distribution*

The cumulative pore size distributions for the Ni-20Cr deposits sprayed at various substrate temperatures are shown in

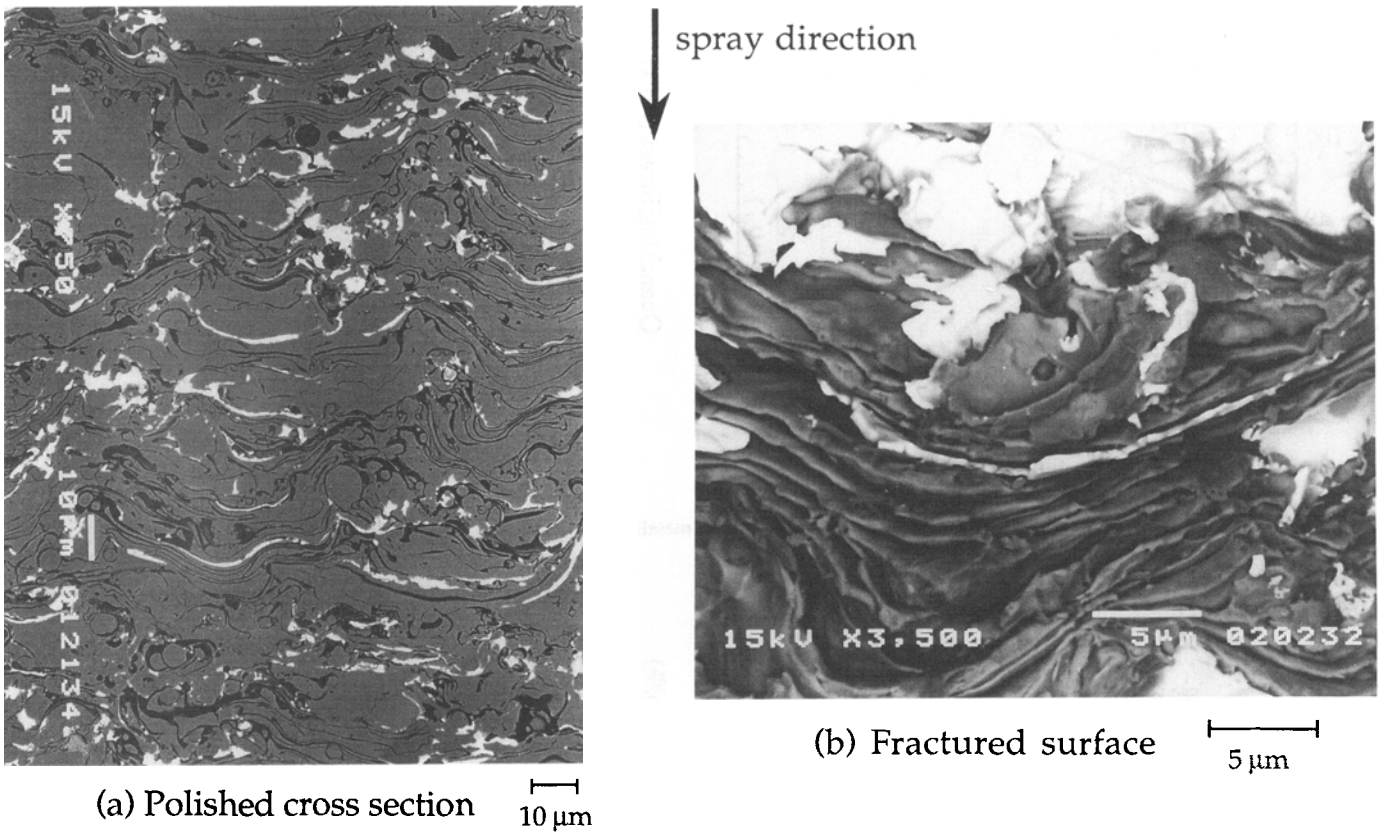

Fig. 8 Back-scattered electron images of polished cross section of Ni-20Cr deposits infiltrated with the Bi alloy (a) and a fractured surface of the sample (b).

Fig. 6. For T_s = 480 K, the majority of the pores were intruded at the pressure corresponding to a radius of around 0.1 μm, and the total open porosity is about 8%. For such a complicated and anisotropic network of porosity in plasma-sprayed deposits, the break-through pressure at which mercury starts to intrude most of the pores tends to be dominated by the size of the narrowest features of the porosity, i.e., interlamellar gaps in this case (Ref 12). As the substrate temperature was raised, both the pore size and porosity decreased. Finally at T_s = 860 K, the Ni alloy deposit became almost impenetrable for mercury even at a pressure over 100 MPa.

For alumina deposits, the pore size distribution and total porosity also decreased with the substrate temperature as shown in Fig. 7, but the deposits remained to be highly penetrable even at T_s = 850 K due to intensive microcracks as shown later.

3.3 *Observation of the Impregnated Specimens*

Figure 8 shows the back-scattered electron images of (a) a polished cross section and (b) a fractured surface of a Ni-Cr deposit, which was sprayed at T_s = 500 K and infiltrated with the Bi alloy. The pores filled with the Bi alloy appear white, the alloy matrix is gray, and the oxides are black on the picture corresponding to their mean atomic weights. On the polished cross section (a), thin and wavy interlamellar gaps as well as chamber-type pores can be seen. Note that the shape of the interlamellar gaps tends to be concave toward the spray direction. This may indicate gas entrapment in these valleys on the surface, for which Fukanuma proposed a mechanism of porosity formation (Ref 15). On the fractured surface (Fig. 8b), a thin sheet (below 1 μm at the periphery) of the Bi alloy between lamellae is clearly seen. Also there are chamber-type pores over a few μm, the size of which could not be measured by mercury porosimetry because they are connected by much narrower interlamellar gaps.

In Fig. 9 polished cross sections of the impregnated Ni alloy deposits for T_s = 500 K and 790 K are shown for comparison. The number of thin interlamellar gaps is significantly reduced at T_s = 790 K. Such information, especially on the interlamellar gaps, could not be obtained by optical microscopy or SEM of the cross sections of metallographically polished specimens without impregnation.

Cross sections of alumina deposits sprayed at two different substrate temperatures and impregnated with chromia are shown for comparison in Fig. 10. Here the pores filled with chromia also appear white, the alumina matrix appears gray, and the pores most likely formed by pull-out during preparation appear black. (Very little closed porosity exists in alumina deposits [Ref 12].) In addition to the two types of pores observed in the Ni-Cr deposits, vertical microcracks are clearly seen in Fig. 10(a). In Fig. 10(b) at T_s = 850 K, the number of horizontal interlamellar gaps significantly decreases, as is the case for Ni-Cr deposits.

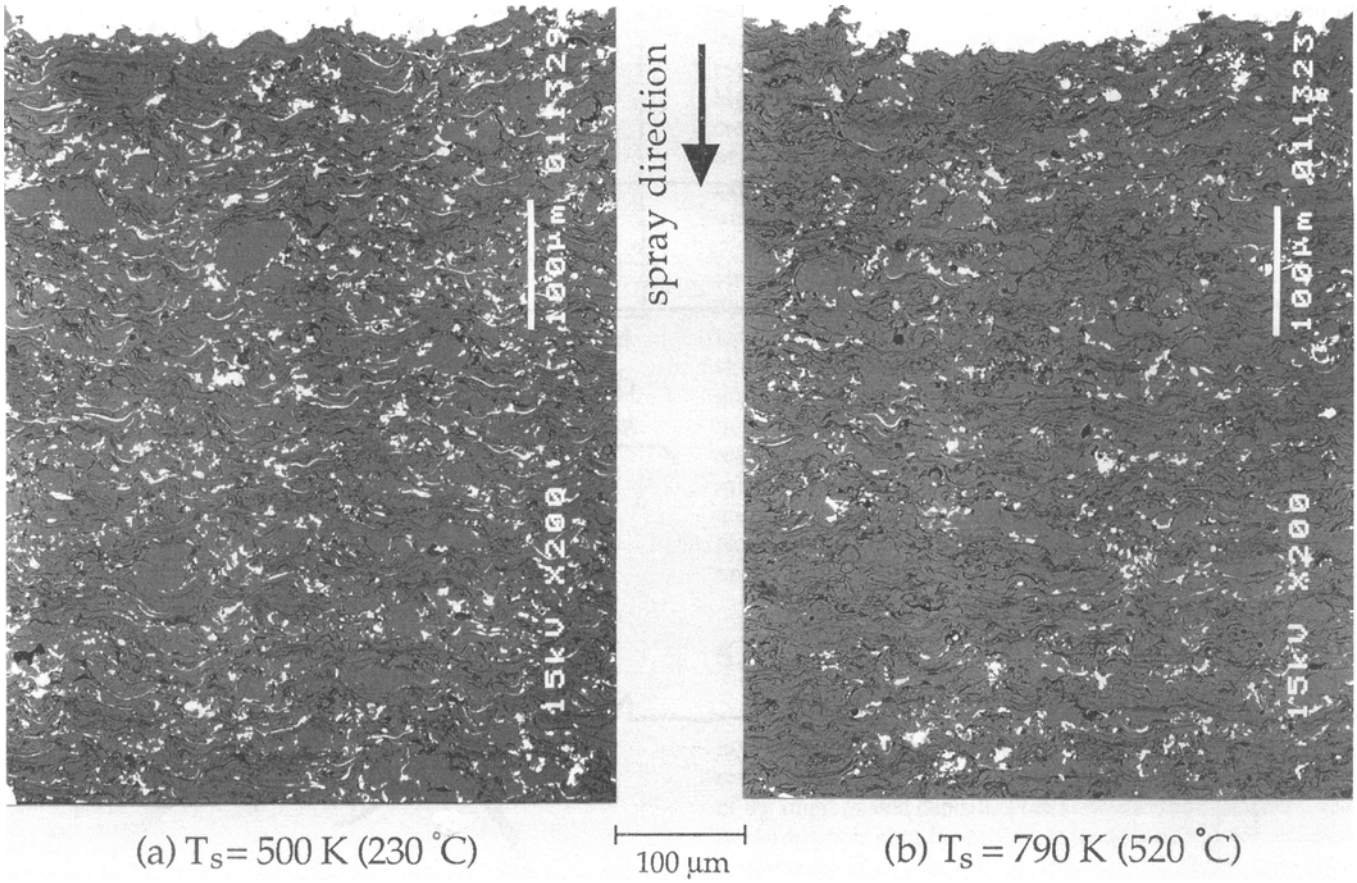

Fig. 9 Back-scattered electron images of polished cross section of Ni-20Cr deposits infiltrated by the Bi alloy. (a) T_S = 500 K. (b) T_S = 790 K.

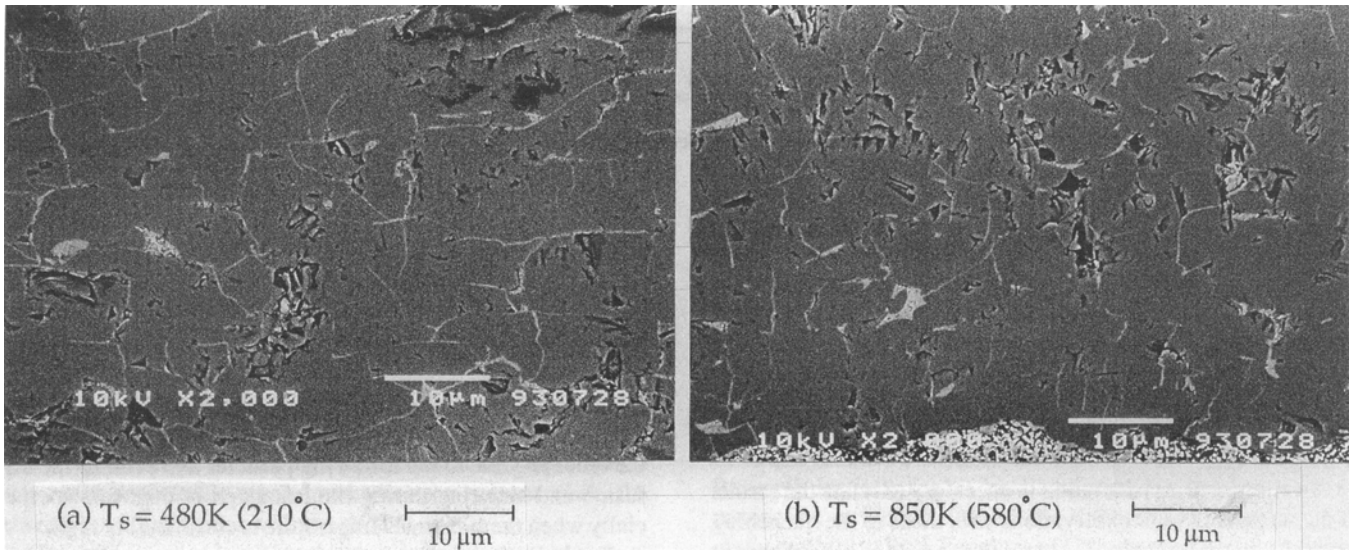

Fig. 10 Back- scattered electron images of polished cross section of alumina deposits treated with chromic acid impregnation technique. (a) T_S = 480 K. (b) T_S = 850 K.

The mercury intrusion porosimetry results and observations of the impregnated deposits indicate that the contact between splats seems to be significantly improved in terms of the ratio of the area of contact to that of noncontact for both the Ni-20Cr and alumina deposits by raising the substrate temperature during deposition from approximately 200 to 600 °C (480 to 870 K).

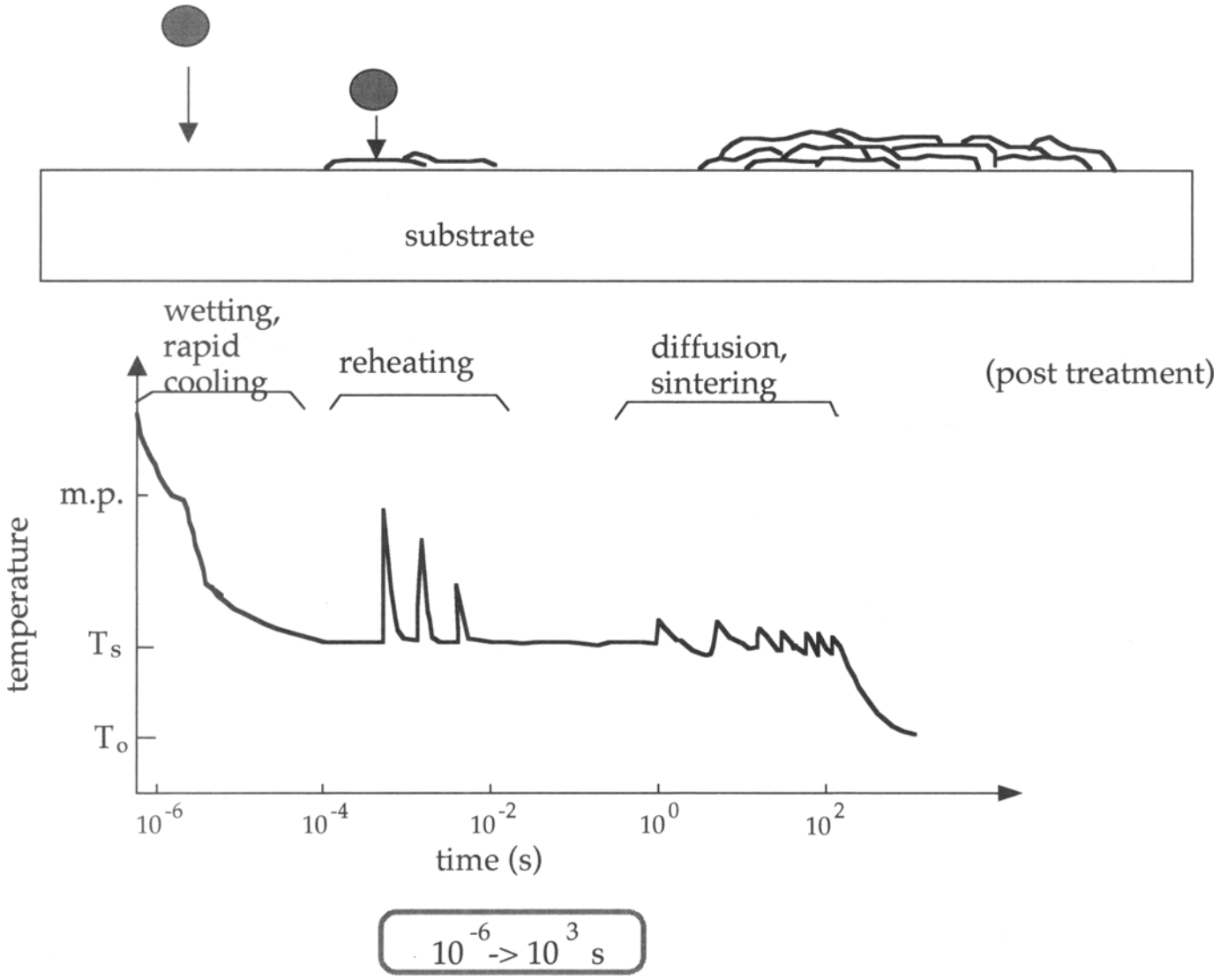

Fig. 11 Schematic diagram of the temperature-time evolution for a powder particle in plasma spraying.

Especially for the Ni-20Cr deposits, the connectivity among the pores becomes so poor that it becomes almost impenetrable for mercury at a pressure over 100 MPa, whereas alumina deposits remain to be highly penetrable due to vertical microcracks.

4. Discussion

An additional consideration is necessary to relate the results of the microstructural observations with those of the quenching stress. If thermal spraying is regarded as a type of heat treatment process for powder materials, it can be characterized by a wide range of time constants in the thermal history of each particle as shown in Fig. 11. It starts with rapid cooling after impact in the time scale of 10^{-6} s, followed by impulsive reheating by the incoming splats thereafter, of which the heat input diminishes quickly as the layers of splats are built up on top. It finally undergoes more moderate periodic heat cycles corresponding to the passages of the spray torch until the desired coating thickness is achieved. The last stage can take well over 10^3 s. In interpreting the structures of sprayed deposits, therefore, keep in mind that the specimen has gone through all these processes. Bonding between splats, for example, is formed at the initial spreading of a molten particle onto a coating surface. Wetting can probably play an important role, but the bonding also can be affected by the reheating due to the following particles and even by the diffusion and sintering during the last stage of deposition, especially when the substrate temperature is considerably high.

To clarify these points, a Ni-Cr deposit sprayed at T_s = 480 K was heated in a furnace at 880 K for 20 minutes, slightly longer than the period of deposition. Then the specimen was examined by the mercury porosimetry, which resulted in the pore size distribution shown in Fig. 12. Even though there was some reduction in both the pore size and total porosity, the effect was far smaller than that of the substrate temperature during deposition. The result, therefore, indicates that the initial contact between

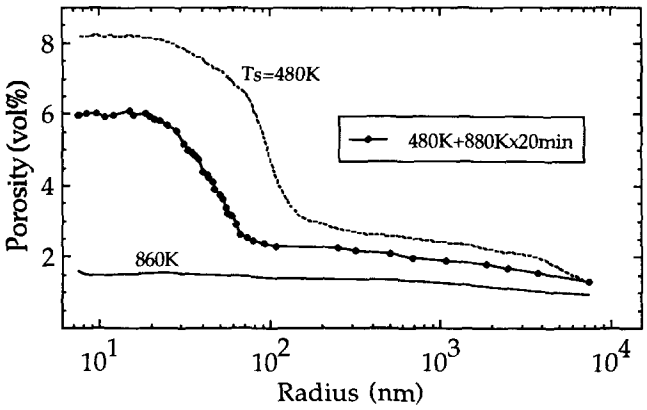

Fig. 12 Effect of heat treatment on the pore size distribution of a Ni-Cr deposit.

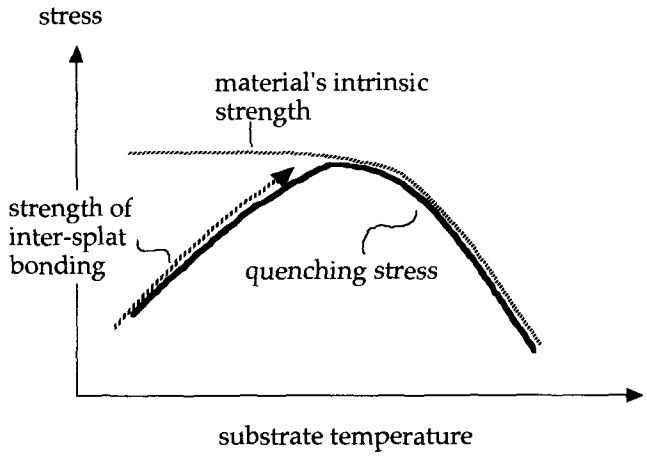

Fig. 13 Schematic diagram for the dependence of quenching stress on substrate temperature and the two regimes governed by different mechanisms.

splats is largely responsible for the observed changes due to a high substrate temperature in the interlamellar bonding within the deposits.

Vardelle et al. reported that the shapes of zirconia splats on polished steel changed dramatically as the substrate temperature was raised from 75 to 150 °C (Ref 16). At 75 °C, splats were irregular and highly disintegrated whereas at 150 °C, they assumed an almost perfect lenticular shape. They also found a significant increase in the cooling rate of the splats on the hotter substrate, which was attributed to enhanced contact between the molten splat and the underlying solid. Even though the temperature range reported is much lower than the present work, the general tendency agrees with the present results.

The effects of substrate temperature on the generation of quenching stress are discussed in the following manner. Consider a splat that just solidified on the surface of a coating and is cooling down towards T_s. Assume the temperature above which the splat material is easily deformable to be $0.6 \times T_m$, where T_m is the melting point of the material. Then the amount of strain effective to the stress generation due to the thermal contraction after solidification may be estimated by $\alpha_d(0.6T_m - T_s)$, where α_d is the thermal expansivity of the material. As the substrate temperature, T_s, is raised, (a) the amount of strain $\alpha_d(0.6T_m - T_s)$ decreases, (b) if the substrate temperature is comparable to or higher than $0.6T_m$, stress relaxation due to plastic deformation or creep can become effective even at T_s, and (c) interfacial sliding of the splat over the underlying coating will be less effective because the contact between the splat and the underlying coating is improved.

Therefore, as shown in Fig. 13, for materials with excellent strength at high temperature, it may be possible to divide the curve of quenching stress into two regimes. In the low-temperature regime, the bonding between splats determines the level of stress to be retained in splats whereas in the high-temperature regime, the intrinsic mechanical properties of the material determine the stress. The situation is more complicated for ceramic materials because the stress within a splat is largely released by microcracks, and the values of the quenching stress measured are the average of the stress in numerously segmented splats. Nevertheless, there is a positive dependence of quenching stress on the substrate temperature.

5. Conclusions

The importance of the intersplat contact in terms of quenching stress and porosity has been examined experimentally. The results of mercury intrusion porosimetry and SEM observation of the impregnated deposits clearly showed that the contact between splats is significantly improved by raising the substrate temperature during deposition from approximately 200 to 600 °C. For the metallic deposits, especially, the enhanced interlamellar contact effectively closes the connectivity of the pores in the deposits, resulting in a highly impenetrable structure. This is considered to be mostly due to a change in the nature of the initial contact between the liquid droplets and the coating surface and hence can play a role in the subsequent quenching phenomena of splats. Better wettability and fluidity of the molten droplets on a hotter surface may be the reasons behind this behavior, but further study is needed. Finally, better intersplat contact is considered to provide a stronger constraint against the contraction of each splat after solidification and can result in significant increase in the values of quenching stress with substrate temperature.

Acknowledgments

Mr. H. Itoh of Nihon Univ. and K. Ikeshima of Shibaura Inst. of Technology are thanked for their sincere cooperation in the experiments. The authors are also grateful to Mr. T. Fukushima of NRIM for his technical assistance and to Dr. T. Senda of Ship Research Institute for his kind advice on the chromic acid impregnation technique. One of the authors (S. Kuroda) is especially grateful to Prof. Fauchais of University of Limoges for his suggestion to contribute a paper to this issue of JTST during S.K.'s stay in Limoges.

References

1. S. Kuroda, T. Fukushima, and S. Kitahara, Simultaneous Measurement of Coating Thickness and Deposition Stress during Thermal Spraying, *Thin Solid Films*, Vol 164, 1988, p 157-163

2. S. Kuroda and T. W. Clyne, The Quenching Stress in Thermally Sprayed Coatings, *Thin Solid Films*, Vol 200, 1991, p 49-66
3. S. Kuroda , T. Fukushima, and S. Kitahara, Generation Mechanisms of Residual Stresses in Plasma-Sprayed Coatings, *Vacuum*, Vol 41 (No. 4-6), 1990, p 1297-1299
4. S. Kuroda and T.W. Clyne, The Origin and Quantification of the Quenching Stress Associated with Splat Cooling during Spray Deposition, *Proc. 2nd Plasma-Technik Symp.*, Vol 3, S. Blum-Sandmeier, H. Eschnauer, P. Huber, and A.R. Nicoll, Ed., Plasma-Technik AG, Wohlen, Switzerland, 1991, p 273-283
5. S.C. Gill and T.W. Clyne, Stress Distributions and Material Response in Thermal Spraying of Metallic and Ceramic Deposits, *Metall. Trans. B*, Vol 21, 1990, p 377-385
6. S.C. Gill and T.W. Clyne, Thermomechanical Modelling of the Development of Residual Stresses during Thermal Spraying, *Proc. 2nd Plasma-Technik Symp.*, Vol 3, S. Blum-Sandmeier, H. Eschnauer, P. Huber, and A.R. Nicoll, Ed., Plasma-Technik AG, Wohlen, Switzerland, 1991, p 227-237
7. S.C. Gill and T.W. Clyne, Investigation of Residual Stress Generation during Thermal Spraying by Continuous Curvature Measurement, *Thin Solid Films*, Vol 250, 1994, p 172-180
8. S.J. Howard and T.W. Clyne, Measurement and Control of the Interfacial Fracture Toughness of Plasma Sprayed Coatings, *Proc. 2nd Plasma-Technik Symp.*, Vol 3, S. Blum-Sandmeier, H. Eschnauer, P. Huber, and A.R. Nicoll, Ed., Plasma-Technik AG, Wohlen, Switzerland, 1991, p 249-261
9. G. Stoney, The Tension of Metallic Films Deposited by Electrolysis, *Proc. R. Soc. (London) A*, Vol 82, 1909, p 172-175
10. A Brenner and S. Senderoff, Calculation of Stress in Electrodeposits from the Curvature of a Plated Strip, *J. Res. Natl. Bur. Stand.*, Vol 42 , 1949, p 105-123
11. W.D. Nix, Mechanical Properties of Thin Films, *Metall. Trans. A*, Vol 20 , 1989, p 2217-2245
12. S. Kuroda, Evaluation of the Pore Structure in Plasma-Sprayed Coatings, to be published in the Proc. 8th Cimtec, Florence, Italy, June, 1994
13. C. Takahashi and T. Senda, Microstructural Analysis of Plasma-Sprayed Alumina Coatings by Image Processing Technique, *J. Jpn. Therm. Spraying Soc.*, Vol 30,1993, p 1-8 (in Japanese)
14. S. Kuroda, H. Fujimori, T. Fukushima, and S. Kitahara, Measurement of Temperature and Velocity of Thermally Sprayed Particles using Thermal Radiation, *Trans. Jpn. Weld. Soc.*, Vol 22, 1991, p 82-89
15. H. Fukanuma, An Analysis of the Porosity Producing Mechanism, *Thermal Spray: International Advances in Coatings Technology*, C. C. Berndt, Ed., ASM International, Materials Park, OH, 1992, p 767-772
16. M. Vardelle, A. Vardelle, A.C. Leger, and P. Fauchais, Influence of the Particle Parameters at Impact on Splat Formation and Solidification in Plasma Spraying Processes, *J. Therm. Spray Technol.*, to be published this issue